

## KINEMATICS OF A HOT MASSIVE ACCRETION DISK CANDIDATE

H. BEUTHER<sup>1</sup> AND A. J. WALSH<sup>2</sup>

Received 2007 July 11; accepted 2007 December 4; published 2007 December 20

### ABSTRACT

Characterizing rotation, infall, and accretion disks around high-mass protostars is an important topic in massive star formation research. With the Australia Telescope Compact Array and the Very Large Array, we studied a massive disk candidate at high angular resolution in ammonia [ $\text{NH}_3(4, 4)$  and  $(5, 5)$ ] tracing the warm disk but not the envelope. The observations resolved at  $\sim 0.4''$  resolution (corresponding to  $\sim 1400$  AU) a velocity gradient indicative of rotation perpendicular to the molecular outflow. Assuming a Keplerian accretion disk, the estimated protostar-disk mass would be high, similar to the protostellar mass. Furthermore, the position-velocity diagram exhibits additional deviation from a Keplerian rotation profile that may be caused by infalling gas and/or a self-gravitating disk. Moreover, a large fraction of the rotating gas is at temperatures  $> 100$  K, markedly different from typical low-mass accretion disks. In addition, we resolve a central double-lobe centimeter continuum structure perpendicular to the rotation. We identify this with an ionized, optically thick jet.

*Subject headings:* stars: early-type — stars: formation — stars: individual (IRAS 18089–1732)

### 1. INTRODUCTION

Outflow and jet studies in high-mass star-forming regions have revealed ample indirect evidence that accretion disks should be common in these regions. However, direct observational characterization of such disks has so far been difficult (e.g., Beuther et al. 2007; Cesaroni et al. 2007). While this is partly caused by the typically large distances and the clustered mode of massive star formation, an additional problem arises because these regions are still deeply embedded within their natal cores—they have visual extinctions of the order 1000—making it difficult to disentangle the dense core emission from the genuine accretion disks. In the past, different molecular line tracers were employed for different massive star-forming regions (e.g., Cesaroni et al. 2007); however, it is interesting to note that for many sources only one or two molecular lines exclusively indicated rotating motions, whereas many other promising spectral lines showed no such signatures (e.g., Beuther 2007). The problem of identifying a reliable massive disk tracer prohibited statistical studies of larger disk samples, until today. Here we present new observations toward the massive disk candidate IRAS 18089–1732 in the high-excitation ammonia lines  $\text{NH}_3(4, 4)$  and  $(5, 5)$ , with lower energy levels of 200 and 295 K, respectively. While the high excitation temperatures ensure that we are not tracing the cold gas envelope but only the warm central regions (e.g., Cesaroni et al. 1998), recent radiative transfer calculations of 3D hydrodynamic massive core simulations indicated that the wavelength regime  $< 100$  GHz should be particularly advantageous to studying the inner disk regions (Krumholz et al. 2007a). This work predicts high dust optical depths at frequencies  $> 100$  GHz, potentially limiting spectral line studies of the central disk in the (sub)millimeter (mm) regime.

The target IRAS 18089–1732 has previously been studied at (sub)mm wavelengths with the Submillimeter Array, and a velocity gradient was identified from east to west, perpendicular to the molecular outflow emanating from the core approximately in the north-south direction (Beuther et al. 2004, 2005).

However, these data did not resolve the velocity pattern of this structure and hence did not allow study of its kinematic properties. The region is located at  $\sim 3.6$  kpc, has a bolometric luminosity of about  $10^{4.5} L_\odot$ , and exhibits several other signs of early massive star formation (e.g., Walsh et al. 1998; Sridharan et al. 2002; Beuther et al. 2002a, 2002b; Williams et al. 2004, 2005; Fuller et al. 2005; Edris et al. 2007).

### 2. OBSERVATIONS

#### 2.1. The Australia Telescope Compact Array (ATCA)

IRAS 18089–1732 was observed in 2007 April with the ATCA in a 1.5 km baseline configuration including antenna 6. The phase reference center was R.A.(J2000)  $18^{\text{h}}11^{\text{m}}51^{\text{s}}.4$ , decl.(J2000)  $-17^\circ 31' 28''.5$ . We observed the  $\text{NH}_3(4, 4)$  and  $(5, 5)$  inversion lines with the frequencies of the main hyperfine components at 24.139 and 24.533 GHz, respectively. The velocity relative to the local standard of rest ( $v_{\text{lsr}}$ ) is  $\sim 33.8$  km  $\text{s}^{-1}$ . Phase and amplitude were calibrated by regular observations of the quasar 1829–207. Bandpass and flux were calibrated with observations of 1741–038 and 1934–638. The spectral resolution of the observations was 62 kHz, corresponding to a velocity resolution of  $\sim 0.8$  km  $\text{s}^{-1}$ . Applying a robust weighting of 0.5, the  $1 \sigma$  rms per 0.8 km  $\text{s}^{-1}$  channel is  $\sim 2.5$  mJy  $\text{beam}^{-1}$ . The synthesized beam is  $2.8'' \times 0.4''$  with a position angle of  $8.5^\circ$ . Because the outflow is in the north-south direction (Beuther et al. 2004) and the expected accretion disk in the east-west direction, the small synthesized beam along the east-west axis is fortunate for the analysis.

#### 2.2. The Very Large Array (VLA)

To improve the beam shape, we observed the same region in 2007 October with the VLA/eVLA hybrid array in an extended configurations (BnA) in the  $\text{NH}_3(5, 5)$  line. Because of mediocre weather conditions and a worse performance of the retrofitted eVLA antennas at high frequencies, we could not usefully include the longest baselines, restricting the data to uv-ranges  $\leq 500$  k $\lambda$ . Bandpass and flux calibration were conducted with 1331+305 and 1733–130. Fast switching between source and phase calibrator 1832–105 were applied to calibrate the phases and amplitudes. The original spectral resolution of 48.8 kHz was smoothed in the final data cube to 1.0 km  $\text{s}^{-1}$ .

<sup>1</sup> Max Planck Institute for Astronomy, Königstuhl 17, 69117 Heidelberg, Germany; beuther@mpia.de.

<sup>2</sup> Centre for Astronomy, James Cook University, Townsville, QLD 4811, Australia; andrew.walsh@jcu.edu.au.

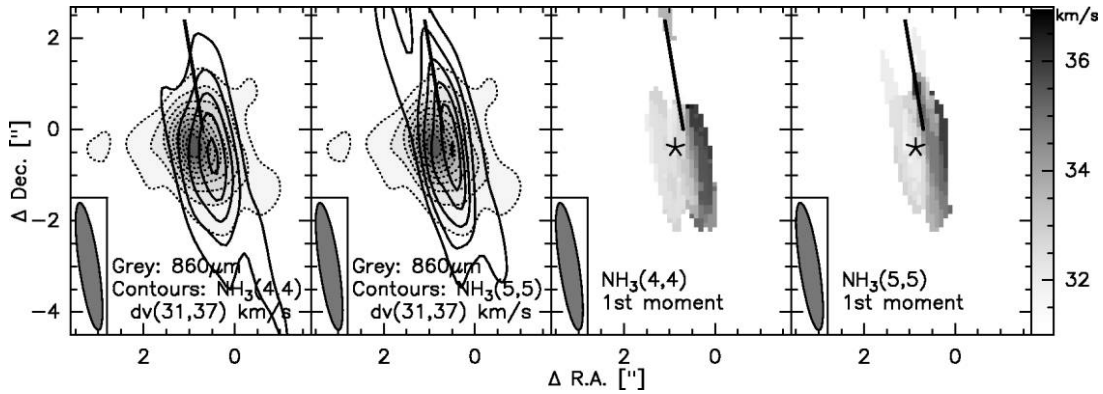


FIG. 1.—The two left panels present in solid contours the NH<sub>3</sub>(4, 4) and (5, 5) emission integrated from 31 to 37 km s<sup>-1</sup>. The gray scale shows the corresponding 860 μm continuum emission (Beuther et al. 2005). The continuum emission is contoured from 10% to 90% (step 10%) of the peak emission of 1.4 Jy beam<sup>-1</sup>. The NH<sub>3</sub> maps are contoured in 3 σ steps with 3 σ values of 3.75 and 3.3 mJy beam<sup>-1</sup> for the (4, 4) and (5, 5) integrated maps, respectively. The two right panels show the corresponding first-moment maps of the NH<sub>3</sub>(4, 4) and (5, 5) spectral line data cubes. The asterisks mark the peak position of the submm continuum emission, and the synthesized beam is shown at the bottom left of each panel. The full line outlines the direction of the outflow as measured in SiO(8–7) (Beuther et al. 2005).

Applying natural weighting and restoring the data with a circular beam (degraded to the larger axis of the fit to the dirty beam), the synthesized beam of these data is 0.47". It was also possible to extract a 1.2 cm continuum map from the line-free part of the spectrum. For this image we included longer baselines as well, and the synthesized beam is 0.26" × 0.19" with a position angle of 84° from north.

### 3. RESULTS AND DISCUSSION

Figure 1 presents a compilation of the ATCA data compared to the submm continuum emission tracing the central dust and gas core (Beuther et al. 2005). As expected, the warm gas observed in the NH<sub>3</sub> lines traces the central core well. However, more interesting is the velocity structure of the region. The two first-moment maps (the intensity-weighted velocities) of the NH<sub>3</sub>(4, 4) and (5, 5) data cubes both exhibit a velocity gradient from east to west, perpendicular to the molecular outflow emanating approximately in the north-south direction (Beuther et al. 2004). The north-south elongation seen in Figure 1 is caused by the nonsymmetric beam shape. To improve on that, we reobserved the source in the NH<sub>3</sub>(5, 5) line with the VLA. Figure 2 presents an integrated and a first-moment map of these data. The velocity gradient in the east-west direction is obvious again. The fact that the NH<sub>3</sub> structure is not flattened could be due to either a viewing angle of the rotating structure close to face-on, or, since the NH<sub>3</sub> features in the north and south are close to the  $v_{\text{lsr}}$ , they may also contain contributions from the ambient core.

In addition to the spectral line data, Figure 2 presents the simultaneously with the VLA observed 1.2 cm continuum map. The centimeter (cm) emission shows a double-lobe structure in the north-south direction with the dip centered on the submm continuum peak. The integrated emission of this double lobe is 7.4 mJy. In combination with the previously observed 3.6 cm flux of 0.9 mJy (Sridharan et al. 2002), the spectral index between these two wavelengths is ~2, consistent with an ionized, optically thick jet (Reynolds 1986). Since the molecular outflow is also in the north-south direction, we identify this double lobe cm continuum emission with the central jet perpendicular to the rotation axis of the gas.

To get a better impression of the velocity field along the inferred rotation axis, Figure 3 shows a position-velocity diagram cut through the submm continuum peak position along

the east-west axis. For this analysis, we use the ATCA NH<sub>3</sub>(4, 4) data because they combine the best signal-to-noise ratio with the highest spectral and angular resolution along the given axis. The velocity gradient is clearly depicted here as well. With a spatial resolution of 0.4" along this axis, the structure with an approximate size of 2" is well resolved and consistent with rotation of a potential massive accretion disk. Furthermore, with a linear resolution of ~1400 AU, these observations allow us, for the first time, to better characterize the kinematics of the rotating structure.

Referring to the relatively simple picture of low-mass accretion disks that are in Keplerian rotation (e.g., Ohashi et al. 1997; Dutrey et al. 2007), we can calculate the rotationally supported binding mass  $M_{\text{rot}}$  for IRAS 18089–1732 assuming equilibrium between the rotational and gravitational force at the outer radius of the disk:

$$M_{\text{rot}} = \frac{\delta v^2 r}{G} \quad (1)$$

$$\Rightarrow M_{\text{rot}} [M_{\odot}] = 1.13 \cdot 10^{-3} \times \delta v^2 [\text{km s}^{-1}] \times r [\text{AU}]. \quad (2)$$

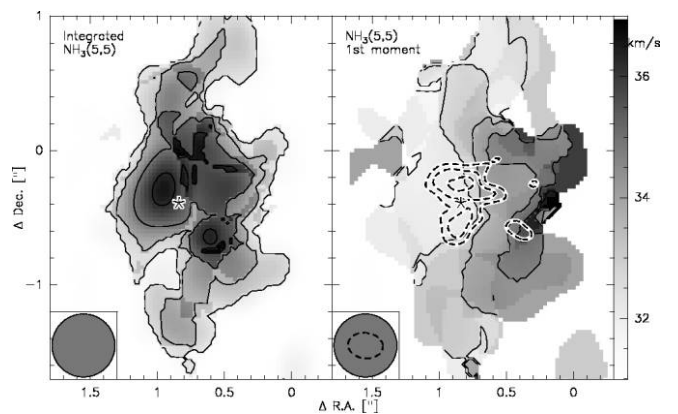


FIG. 2.—The left panel shows the VLA NH<sub>3</sub>(5, 5) emission integrated from 31 to 37 km s<sup>-1</sup> and contoured from 10% to 90% (step 20%) of the peak emission. The right panel presents the corresponding first-moment map contoured from 31.5 to 36.5 km s<sup>-1</sup> (step 1 km s<sup>-1</sup>). The white-black dashed contours show the 1.2 cm continuum emission. Contour levels start at 4 σ and continue in 1 σ steps of 0.28 mJy beam<sup>-1</sup>. The asterisks mark the position of the submm continuum peak (Beuther et al. 2005), and the synthesized beams are shown at the bottom left (NH<sub>3</sub> [gray] and 1.2 cm [dashed] emission).

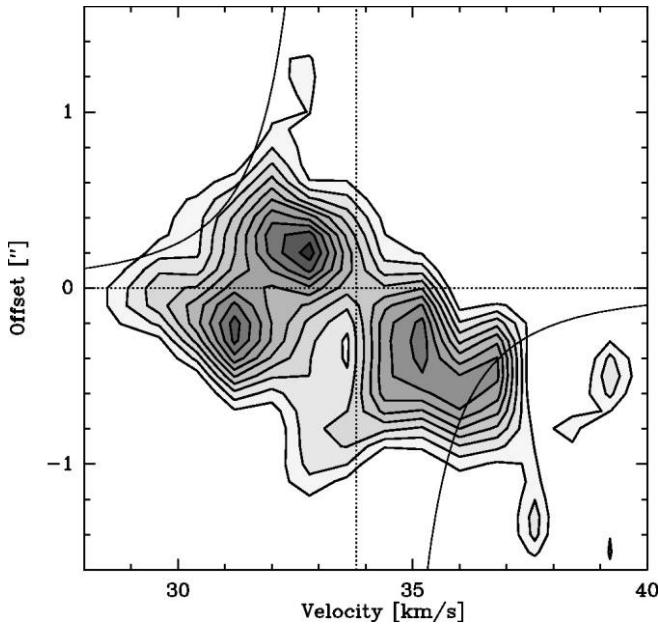


Fig. 3.—Position-velocity diagram of the  $\text{NH}_3(4, 4)$  data through the submm peak position in the east-west direction. The contouring starts at the  $2\sigma$  level and continues in  $1\sigma$  steps ( $1\sigma \sim 2.5 \text{ mJy beam}^{-1}$ ). The dotted lines mark the central position and the systemic velocity. The full line shows a Keplerian rotation curve with a central mass of  $15 M_\odot$ , which obviously fails to fit the data well.

Here  $r$  is the disk radius ( $\sim 1'' \sim 3600 \text{ AU}$ ) and  $\delta v$  half the velocity regime observed in the first-moment maps ( $\sim 3 \text{ km s}^{-1}$ ; Fig. 1). Equations (1) and (2) have to be divided by  $\sin^2(i)$ , where  $i$  is the unknown inclination angle between the disk plane and the plane of the sky ( $i = 90^\circ$  for an edge-on system). With the given values, we can estimate  $M_{\text{rot}}$  to  $\sim 37/[\sin^2(i)] M_\odot$ . This mass estimate is comparable to the core mass estimates from the submm dust continuum emission (about  $45 M_\odot$ ; Beuther et al. 2005).

A different way to assess potential (non-)Keplerian components in the velocity structure is to draw an expected Keplerian velocity profile for a  $15 M_\odot$  protostar on the position-velocity diagram (Fig. 3; for the mass estimate, see the following paragraph). While for blueshifted velocities and positive offsets the position-velocity structure does approximately follow the Keplerian profile, the redshifted emission at negative velocities deviates more strongly from the synthetic profile, even showing super-Keplerian velocities in excess of the Keplerian speed. Furthermore, there are additional components in the position-velocity diagram, for example, the strong peak at ( $31 \text{ km s}^{-1}$ ,  $-0.2''$ ) that does not fit a typical Keplerian disk. How can we explain the non-Keplerian signatures in the rotating structure?

Even at the highest angular resolution (continuum data in Fig. 1), the source remains a single-peaked structure without exhibiting signs of multiplicity. Although massive star formation usually proceeds in a clustered mode, this indicates that most of the bolometric luminosity of  $10^{4.5} L_\odot$  likely stems from the most massive central object. Assuming a main-sequence star, this would give an upper mass limit of  $20 M_\odot$  for the central object. Since the source is likely still in its accretion phase, it has additional accretion luminosity (McKee & Tan 2003; Krumholz et al. 2007b) and the actual protostellar mass may be lower. However, estimating for example the accretion luminosity  $L_{\text{acc}} = GM_*\dot{M}_{\text{acc}}/R_*$  for a star of  $M_* = 15 M_\odot$  with

a radius of  $R_* = 10 R_\odot$  and an accretion rate of  $\dot{M}_{\text{acc}} = 10^{-4} M_\odot \text{ yr}^{-1}$ , one derives an  $L_{\text{acc}}$  of only  $\sim 5 \times 10^3 L_\odot$ . Although especially  $\dot{M}_{\text{acc}}$  and  $R_*$  could both vary by a factor of a few (e.g., Krumholz et al. 2007b), it is unlikely that the accretion luminosity contributes more than a factor of 2 to the overall luminosity. Therefore, we estimate the mass of the central protostar to be likely between 15 and  $20 M_\odot$ . Compared to the mass of the potential protostar/disk system calculated either from the dust continuum emission or estimated via the rotational support assumption, the actual protostellar mass is more than a factor of 2 lower. Hence, a Keplerian supported disk, where the disk mass is negligible compared to the protostellar mass, is not feasible in such a system. Because of the velocity gradient perpendicular to the outflow (Figs. 1 and 2) and the comparatively low velocities compared to molecular outflows, it is unlikely that these features are due to unbound motions, e.g., from the molecular outflow. The more likely interpretation is that we are dealing with a massive rotating structure not in Keplerian rotation.

Candidates for the non-Keplerian contributions are a rotating and infalling envelope and a potentially self-gravitating disk structure. For example, an infalling and rotating envelope produces similar features in the position-velocity diagram like the blueshifted peak at ( $31 \text{ km s}^{-1}$ ,  $-0.2''$ ) in Fig. 3 (see, e.g., Fig. 10 in Ohashi et al. 1997). Such rotating, infalling envelope structures could resemble the proposed larger-scale toroids that are observed toward a small number of even more luminous sources (Cesaroni 2005; Cesaroni et al. 2007). It is expected that such toroidal nonequilibrium structures should be gravitationally unstable, maybe forming companion sources (Kratzer & Matzner 2006; Krumholz et al. 2007b), which then could produce additional kinematic signatures. In a similar direction, Keto & Wood (2006) and Keto (2007) modeled the accretion flow around high-mass stars: in their case, the gas orbits on ballistic trajectories around a point mass (see also Ulrich 1976; Terebey et al. 1984), and the accretion flow appears quasi-spherical at large distances from the star, flattening to a disk at smaller radii owing to conservation of angular momentum (see Fig. 9 in Keto & Wood 2006). Also noteworthy are the redshifted super-Keplerian gas velocities exceeding the Keplerian speed. While sub-Keplerian disks are predicted for disks with significant additional support against gravity than rotation (e.g., magnetic field; Galli et al. 2006), super-Keplerian velocities are expected if the disk contributes a significant fraction of the mass to the protostar-disk system. In this case, the outer disk rotates faster because it feels the gravitational force of the protostar and the inner disk (e.g., Krumholz et al. 2007b and M. R. Krumholz, private communication).

In addition to the kinematic analysis, ammonia is a well-known thermometer for molecular gas (Walmsley & Ungerechts 1983). However, because even these high-excitation lines still have high optical depths ( $\tau > 1$ ), we cannot accurately fit the hyperfine structure of the lines. Therefore, reasonable rotational temperature estimates are not feasible. Nevertheless, the detection of spectral lines with excitation temperatures  $\geq 200 \text{ K}$  implies that the average gas temperatures should exceed  $100 \text{ K}$ , consistent with previous temperature estimates based on  $\text{HCOOCH}_3$  and  $\text{CH}_3\text{CN}$  observations at (sub)mm wavelengths (Beuther et al. 2004, 2005). While the previous (sub)mm temperature estimates were based on data that did not resolve the kinematics of the rotating structure and therefore could be attributed to the disk and/or envelope, the  $\text{NH}_3$  data clearly show that the central rotating structure harbors large amounts of warm gas at temperatures  $> 100 \text{ K}$ . This is markedly different

from typical low-mass disks, where the bulk of the gas is at low temperatures  $<30$  K (Piétu et al. 2007).

#### 4. CONCLUSIONS AND SUMMARY

From an observational point of view, this work shows that high-excitation lines at 1.2 cm wavelengths are well suited to study the kinematics around massive protostars. While massive accretion disk research in recent years has mostly focused on (sub)mm interferometer observations, this may not be the ideal wavelength regime because of high optical depth in the innermost regions (Krumholz et al. 2007a). Although there exist examples of  $\text{NH}_3$  disk studies, these were usually done in the low-excitation lines  $\text{NH}_3(1, 1)$  and  $(2, 2)$  (e.g., Zhang et al. 1998; Beltrán et al. 2006). Such low-energy line observations suffer from contributions of the cold envelope material, and high-excitation  $\text{NH}_3$  observations like those presented here may turn out to be one of the best tracers of the central accretion disks around high-mass protostars. Statistically larger samples have to be investigated this way to base our knowledge on more solid ground.

In summary, these observations disentangle the kinematics, the mass, and the temperature of the rotating structure around a high-mass protostar, identifying a hot massive accretion disk

candidate. The kinematic signatures are different from typical Keplerian velocity profiles known from low-mass star formation. These discrepancies could be produced by larger-scale rotating and infalling toroids or envelopes as well as by self-gravitating structures within the massive accretion disk. The estimated gas temperature is  $>100$  K, which is also significantly larger than average temperatures from low-mass accretion disks. While the angular resolution of  $0.4''$  is very high, corresponding to a projected linear resolution of  $\sim 1400$  AU, we are still not resolving the inner accretion disk regions. Notwithstanding the fact that the larger-scale disklike structure observed here deviates from typical Keplerian disk structures, it may be possible that such structures exist on even smaller scales closer to the central protostar. Future observational tests include high spatial resolution observations with ALMA and the completed eVLA, as well as spatially and spectrally resolved observations of vibrationally excited CO lines observable at mid-infrared wavelengths (e.g., CRIRES on VLT).

We like to thank Fabian Walter and Hendrik Linz for their help with the VLA data. H. B. acknowledges financial support by the Emmy-Noether-Programm of the Deutsche Forschungsgemeinschaft (DFG, grant BE2578).

#### REFERENCES

- Beltrán, M. T., et al. 2006, *Nature*, 443, 427  
 Beuther, H. 2007, in *IAU Symp. 237, Triggered Star Formation in a Turbulent Interstellar Medium*, ed. B. G. Elmegreen & J. Palouš (Cambridge: Cambridge Univ. Press), 148  
 Beuther, H., Churchwell, E. B., McKee, C. F., & Tan, J. C. 2007, in *Protostars and Planets V*, ed. B. Reipurth, D. Jewitt, & K. Keil (Tucson: Univ. Arizona Press), 165  
 Beuther, H., Zhang, Q., Sridharan, T. K., & Chen, Y. 2005, *ApJ*, 628, 800  
 Beuther, H., et al. 2002a, *ApJ*, 566, 945  
 ———. 2002b, *A&A*, 390, 289  
 ———. 2004, *ApJ*, 616, L23  
 Cesaroni, R. 2005, *Ap&SS*, 295, 5  
 Cesaroni, R., Galli, D., Lodato, G., Walmsley, C. M., & Zhang, Q. 2007, in *Protostars and Planets V*, ed. B. Reipurth, D. Jewitt, & K. Keil (Tucson: Univ. Arizona Press), 197  
 Cesaroni, R., Hofner, P., Walmsley, C. M., & Churchwell, E. 1998, *A&A*, 331, 709  
 Dutrey, A., Guilloteau, S., & Ho, P. 2007, in *Protostars and Planets V*, ed. B. Reipurth, D. Jewitt, & K. Keil (Tucson: Univ. Arizona Press), 495  
 Edris, K. A., Fuller, G. A., & Cohen, R. J. 2007, *A&A*, 465, 865  
 Fuller, G. A., Williams, S. J., & Sridharan, T. K. 2005, *A&A*, 442, 949  
 Galli, D., Lizano, S., Shu, F. H., & Allen, A. 2006, *ApJ*, 647, 374  
 Keto, E. 2007, *ApJ*, 666, 976  
 Keto, E., & Wood, K. 2006, *ApJ*, 637, 850  
 Kratter, K. M., & Matzner, C. D. 2006, *MNRAS*, 373, 1563  
 Krumholz, M. R., Klein, R. I., & McKee, C. F. 2007a, preprint (astro-ph/0705.0536)  
 ———. 2007b, *ApJ*, 656, 959  
 McKee, C. F., & Tan, J. C. 2003, *ApJ*, 585, 850  
 Ohashi, N., Hayashi, M., Ho, P. T. P., & Momose, M. 1997, *ApJ*, 475, 211  
 Piétu, V., Dutrey, A., & Guilloteau, S. 2007, *A&A*, 467, 163  
 Reynolds, S. P. 1986, *ApJ*, 304, 713  
 Sridharan, T. K., Beuther, H., Schilke, P., Menten, K. M., & Wyrowski, F. 2002, *ApJ*, 566, 931  
 Terebey, S., Shu, F. H., & Cassen, P. 1984, *ApJ*, 286, 529  
 Ulrich, R. K. 1976, *ApJ*, 210, 377  
 Walmsley, C. M., & Ungerechts, H. 1983, *A&A*, 122, 164  
 Walsh, A. J., Burton, M. G., Hyland, A. R., & Robinson, G. 1998, *MNRAS*, 301, 640  
 Williams, S. J., Fuller, G. A., & Sridharan, T. K. 2004, *A&A*, 417, 115  
 ———. 2005, *A&A*, 434, 257  
 Zhang, Q., Hunter, T. R., & Sridharan, T. K. 1998, *ApJ*, 505, L151